# Electromagnetic wave scattering from conducting self-affine surfaces: an analytic and numerical study

**Ingve Simonsen**

*Unité Mixte CNRS/Saint-Gobain "Surface du Verre et Interfaces," 93303 Aubervilliers Cedex, France and Department of Physics, The Norwegian University of Science and Technology, N-7491 Trondheim, Norway*

**Damien Vandembroucq and Stéphane Roux**

*Unité Mixte CNRS/Saint-Gobain "Surface du Verre et Interfaces," 93303 Aubervilliers Cedex, France*

Received May 26, 2000; accepted September 20, 2000; revised manuscript received October 19, 2000

We derive an analytical expression for the scattering of an *s*-polarized plane wave from a perfectly conducting self-affine one-dimensional surface in the framework of the Kirchhoff approximation. We show that most of the results can be recovered by means of a scaling analysis. We identify the typical slope taken over one wavelength as the relevant parameter controlling the scattering process. We compare our predictions with direct numerical simulations performed on surfaces of varying roughness parameters and confirm the broad range of applicability of our description up to very large roughness. Finally we verify that a nonzero electrical resistivity, provided that it is small, does not invalidate our results. © 2001 Optical Society of America

*OCIS codes:* 290.5880, 240.5770.

## 1. INTRODUCTION

Although it has been studied for more than 50 years,[1] wave scattering from rough surfaces remains a very active field. This constant interest comes obviously from the broad variety of its application domains, which include remote sensing, radar technology, long-range radio-astronomy, surface physics, etc., but from the fundamental point of view, the subject has also shown great vitality in recent years. One may particularly cite the back-scattering phenomena either originating from direct multiple scattering[2–4] or mediated by surface plasmon polaritons.[5–9] Still in the context of single scattering, a large number of studies have also been devoted to the development of reliable analytical approximations.[10–13] In all cases, the efficiency of any analytical approximation relies on a proper description of the surface roughness. In most models the height statistics are assumed to be Gaussian correlated.

In this paper we address the question of wave scattering from rough self-affine metallic surfaces. Since the publication of Mandelbrot's book, *The Fractal Geometry Of Nature*,[14] scale invariance has become a classical tool in the description of physical objects. In the more restricted context of rough surfaces, scale invariance takes the form of self-affinity. Classical examples of rough surfaces obeying this type of symmetry are surfaces obtained by fracture[15] or deposition.[16] More recently it was shown that cold rolled aluminum surfaces[17] could also be successfully described by this formalism. In dealing with wave scattering from rough surfaces, this scale invariance has one major consequence of interest: It is responsible for long range correlations. After early work by Berry,[18] many studies have been conducted on the effects of fractal surfaces on wave scattering. Most of these studies were numerical (see, for example, Refs. 19–27); very few analytical or experimental results have been published. Notable exceptions are due to Jakeman and his collaborators,[28,29] who worked on diffraction through self-affine phase screens in the 1980's and more recently on the characterization of growth surfaces.[30–32] We recently presented a complete analytical solution to the problem of wave scattering from a perfectly conducting self-affine surface[33] in the Kirchhoff approximation. In the following we present a complete derivation of this expression and deduce from it analytical expressions for the width of the specular peak and the diffuse tail. These results are compared with direct numerical simulations. We provide evidence that the crucial quantitative parameter is the slope of the surface taken over one wavelength.

## 2. SCATTERING SYSTEM

The scattering system considered in this paper is depicted in Fig. 1. It consists of vacuum in the region $z > \zeta(x)$ and a perfect conductor in the region $z < \zeta(x)$. The incident plane is assumed to be the $xz$ plane. This system is illuminated from the vacuum side by an *s*-polarized plane wave of frequency $\omega = 2\pi/\lambda$. The angles of incidence and scattering are denoted by $\theta_0$ and $\theta$, respectively, and they are defined positive according to the convention indicated in Fig. 1.

In this paper we will be concerned with $1 + 1$-dimensional self-affine surfaces $z = \zeta(x)$. A surface is said to be self-affine between the scales $\xi_-$ and $\xi_+$ if it remains (either exactly or statistically) invariant in this region under transformations of the form

 

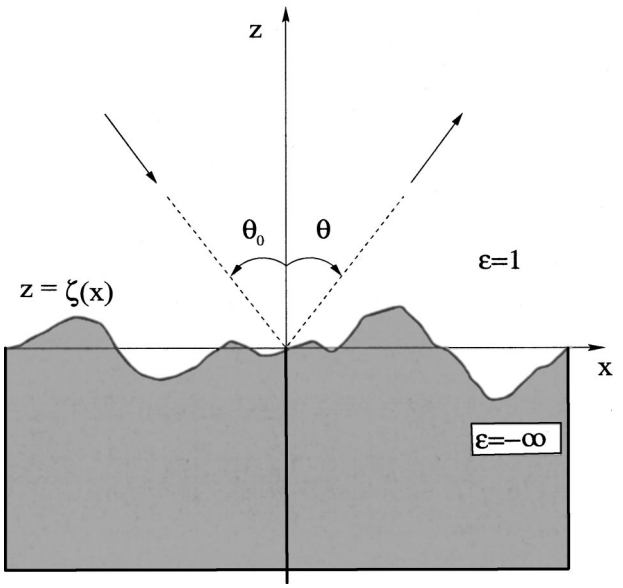


Fig. 1. Scattering geometry considered in this paper.

$$\Delta x \to \mu \Delta x, \tag{1a}$$

$$\Delta \zeta \to \mu^H \Delta \zeta, \tag{1b}$$

for all positive real numbers $\mu$. Here $H$ is the roughness exponent, also known as the Hurst exponent, and it characterizes this invariance. This exponent is usually found in the range from zero to one. A statistical translation of the preceding statement is that the probability $p(\Delta\zeta;\ \Delta x)$ of having a height difference in the range $[\Delta\zeta,\ \Delta\zeta + \mathrm{d}(\Delta\zeta)]$ over the (lateral) distance $\Delta x$ is such that

$$p(\Delta\zeta;\ \Delta x)\mathrm{d}(\Delta\zeta) = p(\mu^H\Delta\zeta;\ \mu\Delta x)\mathrm{d}(\mu^H\Delta\zeta). \tag{2}$$

Simple algebra based on scaling relations (1) gives that the standard deviation of the height differences $\zeta(x + \Delta x) - \zeta(x)$ measured over a window of size $\Delta x$ can be written as

$$\sigma(\Delta x) = l^{1-H}\Delta x^H \tag{3a}$$

and the (mean) slope of the surface as

$$s(\Delta x) = \left(\frac{l}{\Delta x}\right)^{1-H}. \tag{3b}$$

In these equations, $l$ denotes a length scale known as the topothesy. It is defined as $\sigma(l) = l$ [or $s(l) = 1$].

Alternatively, Eq. (3a) can be written in the form

$$\sigma(\Delta x) = \sigma(\lambda)\left(\frac{\Delta x}{\lambda}\right)^H = \lambda s(\lambda)\left(\frac{\Delta x}{\lambda}\right)^H, \tag{4}$$

where we use the wavelength $\lambda$ of the scattering problem as the normalization length. Here $\sigma(\lambda)$ and $s(\lambda)$ are, respectively, the typical height difference and slope over one wavelength as defined by Eqs. (3). Note that we could have used any length scale for the normalization, such as, for instance, the topothesy. However, the choice made here was dictated by the physical problem studied. Using similar scaling arguments, one can show that the power density function of the height profile $\mathcal{P}(k)$ depends on the wave number $k$ as a power law:

$$\mathcal{P}(k) = \left|\int_{-\infty}^{\infty}\zeta(x)\exp(ikx)\mathrm{d}x\right|^2 \propto k^{-1-2H}. \tag{5}$$

In the case of a Gaussian height distribution, the probability $p(\Delta\zeta;\ \Delta x)$ reads as

$$p(\Delta\zeta;\ \Delta x) = \frac{\lambda^{H-1}}{\sqrt{2\pi}s(\lambda)\Delta x^H}\exp\left\{-\frac{1}{2}\left[\frac{\lambda^{H-1}\Delta\zeta}{s(\lambda)\Delta x^H}\right]^2\right\}. \tag{6}$$

The self-affine profile is thus fully characterized by the roughness exponent $H$, the slope $s(\lambda)$ (which is nothing but an amplitude parameter), and the bounds of the self-affine regime $\xi_-$ and $\xi_+$.

Numerous methods have been developed to estimate these parameters (see, for example, Ref. 34); most of them use the expected power-law variation of a roughness estimator computed over spatial ranges of varying size. This roughness estimator can be a height standard deviation, the difference between the maximum and the minimum height, etc. It is also classical to use directly the power density function of the profile. More recently the wavelet analysis has been shown to offer a highly efficient method to compute the roughness exponent of self-affine surfaces.[35]

## 3. SCATTERING THEORY

In the following we consider the scattering of $s$-polarized electromagnetic waves from a one-dimensional, random, Gaussian self-affine surface $z = \zeta(x)$. It will be assumed that the lower limit of the self-affine regime $\xi_-$ is smaller than the wavelength $\lambda$ of the incident wave. For the present scattering system, where the roughness is one dimensional, the complexity of the problem is reduced significantly. The reason is that there is no depolarization, and therefore the original three-dimensional vector scattering problem reduces to a two-dimensional scalar problem for the single nonvanishing second component for the electric field, $\Phi(x, z|\omega) = E_y(x, z|\omega)$, which should satisfy the (scalar) Helmholtz equation

$$\left(\partial_x^2 + \partial_z^2 + \frac{\omega^2}{c^2}\right)\Phi(x, z|\omega) = 0, \tag{7}$$

with vanishing boundary condition on the randomly rough surface $z = \zeta(x)$ and the outgoing wave condition at infinity. In the far-field region, above the surface, the field can be represented as the sum of an incident wave and scattered waves:

$$\Phi(x, z|\omega) = \Phi_0(x, z|\omega) + \int_{-\infty}^{\infty}\frac{\mathrm{d}q}{2\pi}R(q|k) \times \exp[iqx + i\alpha_0(q, \omega)z] \tag{8}$$

where the plane incident wave is given by

$$\Phi_0(x, z|\omega) = \exp[ikx - i\alpha_0(k, \omega)z] \tag{9}$$

and $R(q|k)$ is the scattering amplitude. In the above expressions we have defined

$$\alpha_0(q, \omega) = \sqrt{(\omega/c)^2 - q^2},$$
$$\Re\alpha_0(q, \omega) > 0, \qquad \Im\alpha_0(q, \omega) > 0. \tag{10}$$

Furthermore, the (longitudinal) momentum variables $q$ and $k$ are, in the radiative region, related to the scattering angle and the incident angle by

$$k = \frac{\omega}{c}\sin\theta_0, \tag{11a}$$

$$q = \frac{\omega}{c}\sin\theta, \tag{11b}$$

respectively, so that the $z$ components of the incident and the scattering wave vectors become

$$\alpha_0(k,\omega) = \frac{\omega}{c}\cos\theta_0, \tag{11c}$$

$$\alpha_0(q,\omega) = \frac{\omega}{c}\cos\theta. \tag{11d}$$

The mean differential reflection coefficient (DRC), also known as the mean scattering cross section, is an experimentally accessible quantity. It is defined as the fraction of the total, time-averaged, incident energy flux scattered into the angular interval $(\theta, \theta + d\theta)$. It can be shown to be related to the scattering amplitude by the following expression[36]:

$$\left\langle \frac{\partial R_s}{\partial\theta} \right\rangle = \frac{1}{L}\frac{\omega}{2\pi c}\frac{\cos^2\theta}{\cos\theta_0}\langle |R(q|k)|^2\rangle. \tag{12}$$

Here $L$ denotes the length covered by the self-affine profile as measured along the $x$ direction, and the other quantities were defined earlier in the paper. The angle brackets denote an average over an ensemble of realizations of the rough-surface profiles. Moreover, the momentum variables appearing in Eq. (12) are understood to be related to the angles $\theta_0$ and $\theta$ according to Eqs. (11).

We now impose the Kirchhoff approximation, which consists of locally replacing the surface by its tangential plane at each point and thereafter using the (local) Fresnel reflection coefficient for the local angle of incidence to obtain the scattered field. Notice that dealing with a surface whose scaling invariance range is bounded by a lower cutoff $\xi_-$ does ensure that the tangential plane is well defined at every point. Within the Kirchhoff approximation the scattering amplitude can be expressed as[36]:

$$R(q|k) = \frac{-i}{2\alpha_0(q,\omega)}\int_{-L/2}^{L/2} dx \exp[-iqx - i\alpha_0(q,\omega)\zeta(x)] \times \mathcal{N}_0(x|\omega), \tag{13a}$$

where $\mathcal{N}_0(x|\omega)$ is a source function defined by

$$\mathcal{N}_0(x|\omega) = 2\partial_n\Phi_0(x,z|\omega)|_{z=\zeta(x)}. \tag{13b}$$

Here $\partial_n$ denotes the (unnormalized) normal derivative defined as $\partial_n = -\zeta'(x)\partial_x + \partial_z$.

By substituting the expression for the scattering amplitude, Eq. (13a), into Eq. (12), one obtains an expression for the mean DRC in terms of the source function $\mathcal{N}_0(x|\omega)$: the normal derivative of the total field evaluated on the rough surface. After some straightforward algebra where one takes advantage of the fact that the self-affine surface-profile function $\zeta(x)$ has stationary increments, one obtains the following form for the mean DRC:

$$\left\langle \frac{\partial R_s}{\partial\theta} \right\rangle = \frac{\omega}{2\pi c}\frac{1}{\cos\theta_0}\left(\frac{\cos[(\theta+\theta_0)/2]}{\cos[(\theta-\theta_0)/2]}\right)^2 \times \int_{-L/2}^{L/2} dv \exp\left[ i\frac{\omega}{c}(\sin\theta - \sin\theta_0)v \right]\Omega(v), \tag{14a}$$

where

$$\Omega(v) = \left\langle \exp\left[ -i\frac{\omega}{c}(\cos\theta + \cos\theta_0)\Delta\zeta(v) \right] \right\rangle, \tag{14b}$$

with $\Delta\zeta(v) = \zeta(x) - \zeta(x+v)$. Note that the statistical properties of the profile function, $\zeta(x)$, enters Eqs. (14) only through $\Omega(v)$. With the height distribution $p(\Delta\zeta;\Delta x)$ introduced in Eq. (6), one may now analytically calculate the ensemble average contained in $\Omega(v)$. For a Gaussian self-affine surface one gets

$$\Omega(v) = \int_{-\infty}^{\infty} dz \exp\left[ -i\frac{\omega}{c}(\cos\theta + \cos\theta_0)z \right] p(z;v) = \exp\left\{ -\left[ \frac{\omega}{c}\frac{\cos\theta + \cos\theta_0}{\sqrt{2}} s(\lambda)\lambda^{1-H} v^H \right]^2 \right\}. \tag{15}$$

By making the change of variable in Eq. (14),

$$u = v\left[ \frac{\omega}{c}\frac{\cos\theta + \cos\theta_0}{\sqrt{2}} s(\lambda)\lambda^{1-H} \right]^{1/H}, \tag{16}$$

and letting the length of the profile extend to infinity, $L \to \infty$, one finally obtains the following expression for the mean DRC:

$$\left\langle \frac{\partial R_s}{\partial\theta} \right\rangle = \frac{s(\lambda)^{-1/H} a^{-(1/H-1)}}{\sqrt{2}\cos\theta_0}\frac{\cos\dfrac{\theta+\theta_0}{2}}{\cos^3\dfrac{\theta-\theta_0}{2}} \times \mathcal{L}_{2H}\left( \frac{\sqrt{2}\tan\dfrac{\theta-\theta_0}{2}}{a^{1/H-1}s(\lambda)^{1/H}} \right), \tag{17a}$$

where

$$a = 2\pi\sqrt{2}\cos\frac{\theta+\theta_0}{2}\cos\frac{\theta-\theta_0}{2}, \tag{17b}$$

and $(0 < \alpha \leqslant 2)$

$$\mathcal{L}_\alpha(x) = \frac{1}{2\pi}\int_{-\infty}^{\infty} dk \exp(ikx)\exp(-|k|^\alpha). \tag{17c}$$

The quantity $\mathcal{L}_\alpha(x)$ is known as the centered symmetric Lévy stable distribution of index (or order) $\alpha$.[37] This distribution can be expressed only in closed form for some particular values of $\alpha$: $\alpha = 1$ and $\alpha = 2$ correspond to the Cauchy–Lorentzian and the Gaussian distributions

respectively; $\mathcal{L}_{1/2}$ and $\mathcal{L}_{1/3}$ can be expressed from special functions. When the $\alpha$ index in the Lévy distribution $\mathcal{L}_\alpha(x)$ is lowered from its upper value $\alpha = 2$ (Gaussian distribution), the resulting distribution develops a sharper peak at $x = 0$ while at the same time its tails become fatter. It is interesting to note from Eqs. (17) that the wavelength, $\lambda = 2\pi c/\omega$, comes into play only through the slope $s(\lambda)$. The behavior of the scattered intensity is thus determined entirely by this typical slope $s(\lambda)$ and the roughness exponent $H$.

In Fig. 2 we show the mean DRC as obtained from Eqs. (17) for Hurst exponent $H = 0.7$ and different values of the slope $s(\lambda)$ ranging from 0.016 to 0.25. The angles of incidence were $\theta_0 = 0°$ [Fig. 2(a)] and 50° [Fig. 2(b)]. It is observed from these figures that as the amplitude parameter $s(\lambda)$ is decreased while the other parameters are kept fixed, the portion of the scattered intensity scattered diffusely is reduced, while the power-law behavior found for the nonspecular directions survives independently (within single scattering) of the amount of light scattered specularly. Furthermore, as the Hurst exponent is decreased (results not shown), thereby making the topography rougher at small scale, the mean DRC gets a larger contribution from diffusely scattered light. This is a direct consequence of the properties of the Lévy distribution mentioned above.

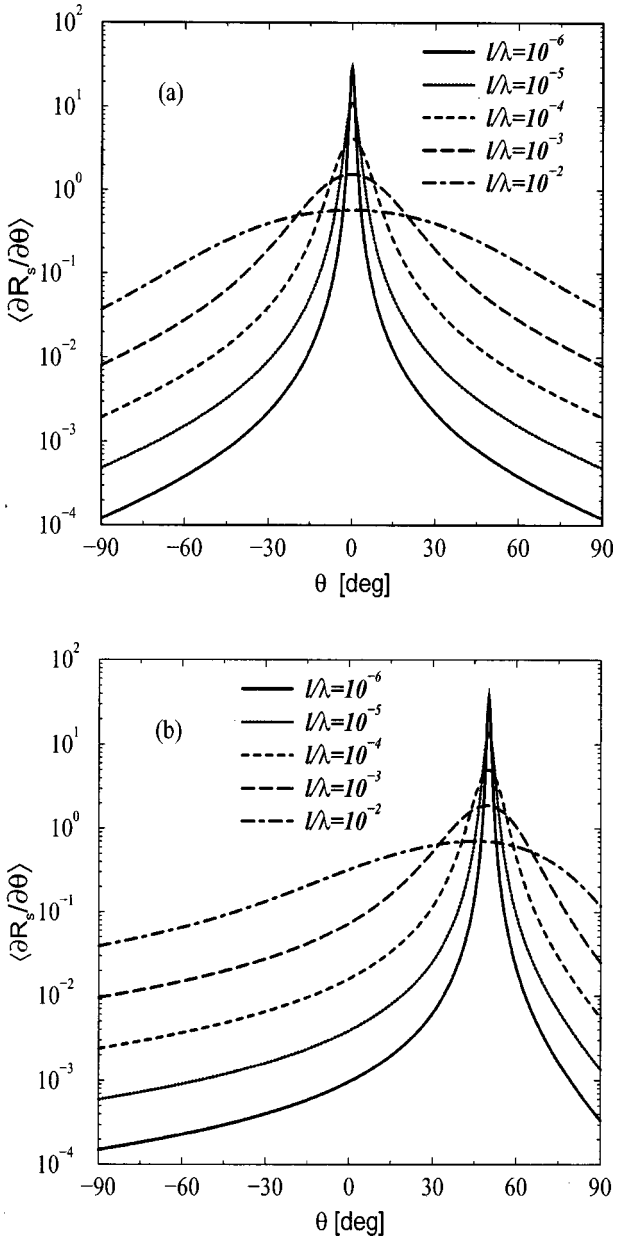


Fig. 2. Mean DRC $\langle \partial R_s/\partial\theta \rangle$ versus scattering angle $\theta$ for a perfectly conducting self-affine surface. The plotted curves are the prediction of Eqs. (17). The Hurst exponent in all cases is $H = 0.7$, and the topothesies $l$ range from $l = 10^{-2}\lambda$ [$s(\lambda) = 0.016$] down to $10^{-6}\lambda$ [$s(\lambda) = 0.25$], as indicated in the figures. The incident angles were (a) $\theta_0 = 0°$ and (b) $\theta_0 = 50°$.

In order to consider the features of the mean DRC, which can be seen in Fig. 2, we now discuss the behavior of the specular and diffuse contribution to $\langle \partial R_s/\partial\theta \rangle$, i.e., close to and far away from the scattering angle $\theta = \theta_0$.

### A. Specular Contribution

We start by considering the specular contribution to the mean DRC. This is done by taking advantage of the asymptotic expansion of the Lévy distribution around zero[38]:

$$\mathcal{L}_\alpha(x) = \frac{1}{\pi\alpha}\Gamma\left(\frac{1}{\alpha}\right)\left[1 - \frac{\Gamma(3/\alpha)}{2\Gamma(1/\alpha)}x^2\right] + \mathcal{O}(x^4). \quad (18)$$

By substituting this expression into Eqs. (17), one finds that the mean DRC around the specular direction $\theta = \theta_0$ should behave as follows ($\delta\theta \ll 1$):

$$\left\langle \frac{\partial R_s}{\partial\theta} \right\rangle\Bigg|_{\theta=\theta_0+\delta\theta} = \frac{\Gamma(1/2H)}{2\sqrt{2}\pi H(2\sqrt{2}\pi\cos\theta_0)^{1/H-1}s(\lambda)^{1/H}} \times \left\{1 + \delta\theta\frac{1-2H}{2H}\tan\theta_0 + \frac{(\delta\theta)^2}{4} \times \left[\frac{1}{H} - \frac{(2H-1)(1-H)}{2H^2}\tan^2\theta_0 - \frac{\Gamma(3/2H)}{\Gamma(1/2H)(2\sqrt{2}\pi\cos\theta_0)^{2/H-2}s(\lambda)^{2/H}}\right]\right\}. \quad (19)$$

From this expression it follows that the amplitude of the specular peak should scale as

$$\left\langle \frac{\partial R_s}{\partial\theta} \right\rangle\Bigg|_{\theta=\theta_0} \simeq \frac{\Gamma(1/2H)}{2\sqrt{2}\pi H(2\sqrt{2}\pi\cos\theta_0)^{1/H-1}s(\lambda)^{1/H}} \quad (20)$$

and that the peak's half-width at half-maximum, $w$, should be given by

$$w(H, s(\lambda), \theta_0) \simeq 2\left[\frac{\Gamma(1/2H)}{\Gamma(3/2H)}\right]^{1/2}(2\sqrt{2}\pi\cos\theta_0)^{1/H-1} \times s(\lambda)^{1/H}. \quad (21)$$

It is worth noting that in the above expression the width of the specular peak depends on the wavelength $\lambda$

via the typical slope over one wavelength $s(\lambda)$. In the case of Gaussian correlations, there would have been no dependence on the wavelength, the peak width $w$ being simply proportional to the ratio $\sigma/\tau$, root mean square (RMS) roughness over correlation length.

In order to test the quality of the specular expansion, Eq. (19), we show in Fig. 3 a comparison of this expression with the full single-scattering solution obtained from Eqs. (17) for a surface of roughness exponent $H = 0.7$ and of slope over the wavelength $s(\lambda) = 0.063$ ($l = 10^{-4}\lambda$) in the case of normal incidence. The amplitude of the specular peak is seen to be nicely reproduced, but this expansion is valid only within a rather small angular interval around the specular direction $\theta = \theta_0$.

It is interesting to note that in the case of a nonzero angle of incidence, $\theta_0 \neq 0°$, the specular peak is shifted slightly away from its expected position $\theta = \theta_0$ owing to the presence of a nonvanishing term in Eq. (19) that is linear in $\delta\theta$. In this case the apparent specular peak is located at $\theta = \theta_0 + \Delta\theta_0$, where $\Delta\theta_0 (\Delta\theta_0 \sim w^2 \ll w)$ scales as

$$\Delta\theta_0 \simeq -\frac{1-2H}{H}\frac{\Gamma(1/2H)}{\Gamma(3/2H)} \times \tan\theta_0 (2\sqrt{2}\pi\cos\theta_0)^{2/H-2} s(\lambda)^{2/H} \simeq \frac{1-4H}{4H}\tan\theta_0 w^2[H, s(\lambda), \theta_0]. \quad (22)$$

Such a shift has not, to our knowledge, been reported earlier for non-self-affine (or nonfractal) surfaces. Hence, because of the self-affinity of the random surface, we predict a shift, $\Delta\theta_0$, in the specular direction in comparison with its expected position at $\theta = \theta_0$. Notice that this shift vanishes for a Brownian random surface ($H = 1/2$). Moreover, for a persistent surface-profile function ($H > 1/2$) the shift is negative, whereas it becomes positive for an antipersistent profile ($H < 1/2$). Unfortunately, the specular shift $\Delta\theta_0$ is probably too small to be observable experimentally for realizable self-affine parameters.

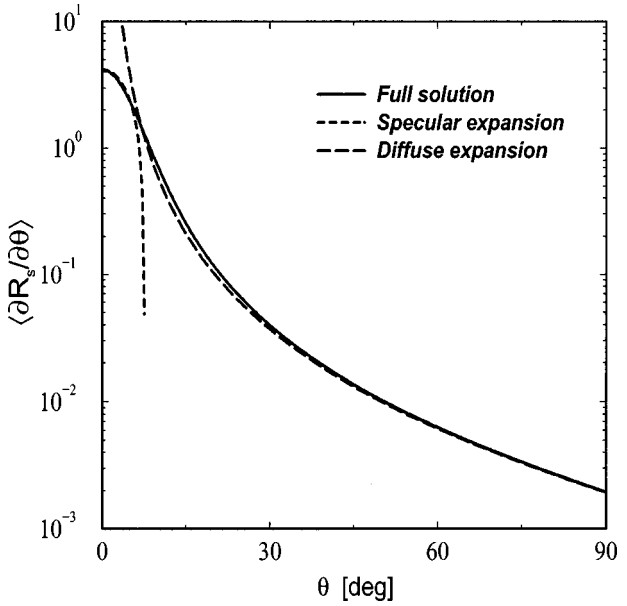


Fig. 3. Full single-scattering solution (solid curve), Eqs. (17), for the mean differential reflection coefficient versus scattering angle $\theta$ for a perfectly conducting self-affine surface compared with its specular (short dashed curve) and diffuse (long dashed curve) expansions as given by relations (19) and (24), respectively. The surface parameters used were $H = 0.7$ and $l = 10^{-4}\lambda$ [$s(\lambda) = 0.063$], and the light was incident normally onto the rough surface.

### B. Diffuse Component

We now focus on the diffuse component of the mean differential reflection coefficient, i.e., the region where $\theta$ is far away from $\theta = \theta_0$. Now, using the expansion of the Lévy distribution at infinity (the Wintner development),[38]

$$\mathcal{L}_\alpha(x) = \frac{\Gamma(1+\alpha)}{\pi|x|^{1+\alpha}}\sin\left(\frac{\alpha\pi}{2}\right) + \mathcal{O}\left(\frac{1}{|x|^{1+2\alpha}}\right), \quad (23)$$

we get the following expression for the diffuse component of the mean DRC ($\theta \neq \theta_0$)

$$\left\langle \frac{\partial R_s}{\partial\theta} \right\rangle \simeq \frac{\Gamma(1+2H)\sin(\pi H)}{(4\pi)^{2H-1}}\frac{s(\lambda)^2}{\cos\theta_0}\frac{\left|\cos\frac{\theta+\theta_0}{2}\right|^{3-2H}}{\left|\sin\frac{\theta-\theta_0}{2}\right|^{1+2H}}. \quad (24)$$

In Fig. 3 the above expression is compared with the prediction of Eqs. (17). We observe an excellent agreement for angular distances larger than 10°. Moreover, it should be noticed from Eq. (24) that the mean DRC is predicted to decay as a power law of exponent $-1-2H$ as we move away from the specular direction. For smooth surfaces (corresponding to small values of $s(\lambda)$) this behavior results directly from a perturbation approach where the scattered intensity is derived directly from the power density function of the surface. As shown above, in the case of self-affine surfaces the latter is a power law of exponent $-1-2H$. Our results extend, then, the validity of this power-law regime to steeper surfaces.

## 4. SCALING ANALYSIS

It is interesting that most of the nontrivial scaling results derived above can be retrieved through simple dimensional arguments. Let us examine the intensity scattered in the direction $\theta$; in a naïve Huygens framework two different effects will compete to destroy the coherence of two source points on the surface: (1) the angular difference separating $\theta$ from the specular direction and (2) the roughness. Considering two points separated by a horizontal distance $\Delta x$ and a vertical distance $\Delta z$, we can define the retardation that is due to these two effects:

$$\Delta c_{\text{ang}} = (\sin\theta - \sin\theta_0)\Delta x,$$

$$\Delta c_{\text{rough}} = (\cos\theta + \cos\theta_0)\Delta z.$$

This allows us to define two characteristic (horizontal) lengths $\delta_{\text{ang}}$ and $\delta_{\text{rough}}$ of the scattering system corresponding to the distances between two points of the surface such that $\Delta c_{\text{ang}}$ and $\Delta c_{\text{rough}}$ are equal to the wavelength $\lambda$. Taking into account the self-affine character of the surface, we get

$$\delta_{\text{ang}} = \frac{\lambda}{\sin\theta - \sin\theta_0},$$

$$\delta_{\text{rough}} = \frac{\lambda}{(\cos\theta + \cos\theta_0)^{1/H}} s(\lambda)^{-1/H}.$$

The coherence length on the surface depends on the relative magnitude of these two characteristic lengths. For scattering angles close to the specular direction, we have $\delta_{\text{rough}} \ll \delta_{\text{ang}}$ and for large scattering angles $\delta_{\text{ang}} \leqslant \delta_{\text{rough}}$, and the diffuse tail is controlled by the angular distance to the specular direction. In general we can evaluate the competition of these two effects and their consequences on the scattering cross section by the simple ratio of the two characteristic lengths:

$$\chi = \frac{\delta_{\text{rough}}}{\delta_{\text{ang}}} = \frac{\sin\theta - \sin\theta_0}{(\cos\theta + \cos\theta_0)^{1/H}} s(\lambda)^{-1/H}.$$

We can then describe our scattering system with this unique variable $\chi$, which takes into account the incidence and scattering directions, the roughness parameters of the surface, and the wavelength. A direct application is the determination of the angular width $w$ of the specular peak. The transition between the specular peak and the diffuse tail is simply defined by $\chi = 1$, which leads to

$$w \simeq [2s(\lambda)]^{1/H} (\cos\theta_0)^{1/H-1},$$

which is identical to the exact result (21) apart from a numerical constant. Assuming that most of the intensity is scattered within the specular peak, we obtain through energy conservation:

$$\left\langle \frac{\partial R_s}{\partial\theta} \right\rangle \Bigg|_{\theta=\theta_0} \simeq \frac{1}{w} \simeq [2s(\lambda)]^{-1/H} (\cos\theta_0)^{1-1/H}.$$

Neglecting the numerical constants, we can thus rewrite the scattering cross section as

$$\left\langle \frac{\partial R_s}{\partial\theta} \right\rangle = \frac{(\cos\theta_0)^{1-1/H}}{s(\lambda)^{1/H}} \Psi(\chi).$$

When approaching the specular direction, we note that $\delta_{\text{ang}}$ diverges, whereas $\delta_{\text{rough}}$ saturates at a finite value independent of the angular direction. In this specular direction, the scattering process is thus controlled by only the latter length and does not depend on the ratio $\chi = \delta_{\text{rough}}/\delta_{\text{ang}}$. This imposes that

$$\Psi(\chi) \simeq 1, \qquad (\chi \ll 1).$$

The argument $\chi$ being inversely proportional to the quantity $s(\lambda)^{1/H}$, which is nothing but a roughness amplitude parameter, the behavior of $\Psi$ for large arguments can be found by matching our expression to the limit of very smooth surfaces. In this limit a simple perturbation approach leads to

$$\left\langle \frac{\partial R_s}{\partial\theta} \right\rangle \propto \mathcal{P}\left[\frac{2\pi}{\lambda}(\sin\theta - \sin\theta_0)\right],$$

where $\mathcal{P}$ is the power density function of the height profile. In the case of a self-affine profile of roughness exponent $H$, we have $\mathcal{P}(k) \propto k^{-1-2H}$. One can verify that this can be consistent only with the same power-law behavior for $\Psi$:

$$\Psi(\chi) \propto \chi^{-1-2H}, \qquad (\chi \gg 1).$$

## 5. NUMERICAL SIMULATION RESULTS AND DISCUSSION

The results obtained in the previous sections were all based on the Kirchhoff approximation and will therefore be accurate only in cases in which single scattering is dominating. In this section, however, we will therefore no longer restrict ourselves to single scattering but instead will include any higher-order scattering process. This is accomplished by a rigorous numerical-simulation approach that will be described below. This approach will also serve as an independent check of the correctness of the analytic results [Eqs. (17)] and the results that can be derived therefrom. Furthermore, it will provide valuable insight into which part of the parameter space is dominated by single-scattering processes and thus where formulas (17) can be used with confidence.

The rigorous numerical-simulation calculations for the mean DRC were performed for a plane incident *s*-polarized wave scattered from a perfectly conducting rough self-affine surface. Such simulations were done by the now quite standard extinction theorem technique.[36] This technique amounts to using Green's second integral identity to write down the following inhomogeneous Fredholm equation of the second kind for the source function $\mathcal{N}(x|\omega)$ (see Refs. 39 and 40):

$$\mathcal{N}(x|\omega) = 2\mathcal{N}_0(x|\omega) - 2\mathcal{P}\int \mathrm{d}x' \times \partial_n G_0(x, z|x', z')|_{z'=\zeta(x')} \mathcal{N}(x'|\omega). \quad (25a)$$

In this equation

$$\mathcal{N}(x|\omega) = \partial_n \Phi(x, z|\omega)|_{z=\zeta(x)}, \quad (25b)$$

where $\partial_n = -\zeta'(x)\partial_x + \partial_z$ is the (unnormalized) normal derivative of the *total* electric field $\Phi = E_y$ evaluated on the randomly rough self-affine surface, $\mathcal{N}_0(x|\omega)$ has been defined earlier in the paper as the normal derivative of the incident field, and $\mathcal{P}$ is used to denote the principal part of the integral. Moreover, $G_0(x, z|x', z')$ is the (two-dimensional) free-space Green's function defined by

$$G_0(x, z|x', z') = i\pi H_0^{(1)}\left(\frac{\omega}{c}|\mathbf{r} - \mathbf{r}'|\right), \quad (25c)$$

where $\mathbf{r} = (x, z)$, $\mathbf{r}' = (x', z')$ and $H_0^{(1)}(x)$ denotes the zeroth-order Hankel function of the first kind.[41] By taking advantage of Eq. (13a), which relates the scattering amplitude to the normal derivative of the total field on the random surface, the scattering amplitude can easily be calculated and from there the mean differential reflection coefficient. It should be noticed that the Kirchhoff approximation used in Section 4 to obtain the analytical results [Eqs. (17)] is obtained from Eq. (25a) by neglecting the last (integral) term, which represents multiple scattering. By using a numerical quadrature scheme,[42] one can solve the integral equation Eq. (25a) for any given re-

alization of the surface profile $\zeta(x)$. From the knowledge of $\mathcal{N}(x|\omega)$ one might then easily calculate the mean DRC.

Randomly rough Gaussian self-affine surfaces of a given Hurst exponent were generated by the Fourier filtering method[43] [see Eq. (5)], i.e., in Fourier space, to filter complex Gaussian random uncorrelated numbers by a decaying power-law filter of exponent $-H - 1/2$ and thereafter transforming this sequence into real space. We then adjusted the topothesies (or slopes) of the surfaces to the desired values $l$ by taking advantage of Eqs. (3). This was done by first calculating the topothesy $l_0$ of the original surface over its total length and thereafter rescaling the profile by $(l_0/l)^{1-H}$, where $l$ is the desired topothesy. In order to have enough statistical information to be able to calculate a well-defined topothesy $l_0$, we in fact used a window size slightly smaller than the total length of the surface.

By the methods just described we performed rigorous numerical simulations for the mean DRC, $\langle \partial R_s/\partial\theta \rangle$, in the case of an *s*-polarized plane incident wave of wavelength $\lambda = 2\pi c/\omega = 612.7\,\text{nm}$ that is scattered from a perfectly conducting self-affine surface characterized by the Hurst exponent $H$ and the topothesy $l$. For all simulation results shown, the length of the surface was $L = 100\lambda$ and the spatial discretization length was $\Delta x \simeq \lambda/10$. All simulation results presented were averaged over $N_\zeta = 1000$ surface realizations (or more). Furthermore, in order to check the quality of the numerical simulations, we checked both reciprocity and unitarity for all simulation results. We found for all cases considered that the reciprocity was satisfied within the noise level of the calculations, and the unitarity was fulfilled within an error of a fraction of a percent.

In Fig. 4 the mean DRC's for surfaces characterized by the parameters $H = 0.7$ and $l = 10^{-4}\lambda$ [$s(\lambda) = 0.063$] are presented. The angles of incidence of the light were $\theta_0 = 0°$ and 50°, as indicated in the figures. The solid curves represent the numerical (multiple-scattering) simulation results, and the dashed curves are the (single-scattering) prediction of Eqs. (17). As can be seen from Fig. 4(a), the correspondence is quite good between the analytic results and those obtained from the numerical simulations. To allow a better comparison for large scattering angles, we present in Fig. 4(b) the results of Fig. 4(a) but now in a linear-log scale. From this figure it is apparent that for the largest scattering angles there are some disagreements between the analytic and the numerical results. The analytic results tend to overestimate the mean DRC in these regions. This discrepancy stems from the fact that multiple scattering is not included in the analytical results. Part of the light that according to single scattering would have been scattered into large scattering angles is now due to multiple-scattering processes, scattered back into smaller angles. This results in *smaller* values for $\langle \partial R_s/\partial\theta \rangle$ for the largest scattering angles. Since the unitarity condition, $\int_{-\pi/2}^{\pi/2} \langle \partial R_s/\partial\theta \rangle \mathrm{d}\theta = 1$, is satisfied for a perfectly reflecting surface, this large-angle reduction of the mean DRC has to be compensated by an increase for other scattering angles. In the case of normal incidence ($\theta_0 = 0°$), say, this increase can be seen in the region near $|\theta| \sim 25°$, where the numerical simulation results are larger than the corresponding single-scattering results. The same behavior can be observed for an angle of incidence of 50°.

We give in Fig. 5 the numerical simulation results for five different values of the topothesy ranging from $l = 10^{-6}\lambda$ [$s(\lambda) = 0.016$] to $10^{-2}\lambda$ [$s(\lambda) = 0.25$]. These multiple-scattering results should be compared with the results of Fig. 2, which show the corresponding curves obtained from Eqs. (17). The roughness exponent used in the simulations leading to the results of Fig. 5 was in all

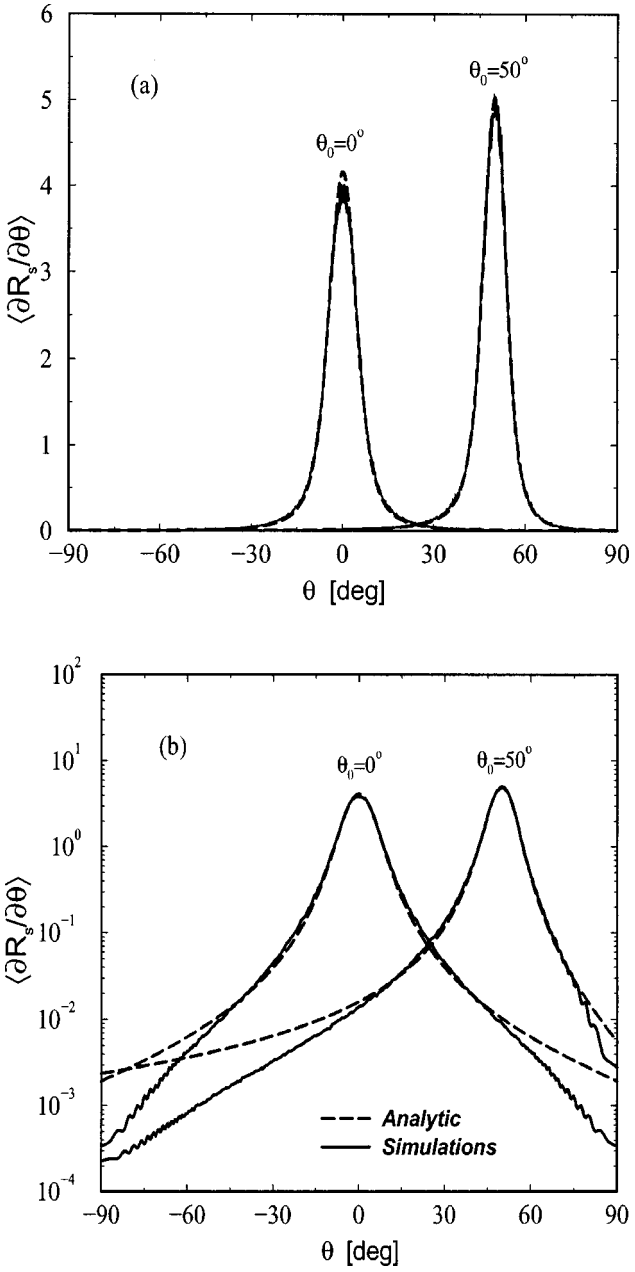


Fig. 4. Comparison plotted in (a) linear and (b) linear-log scale of the mean DRC $\langle \partial R_s/\partial\theta \rangle$ versus scattering angle $\theta$ for a perfectly conducting self-affine surface obtained by a rigorous numerical-simulation approach (solid curves) and therefore including all possible multiple-scattering processes, and the single-scattering results obtained from Eqs. (17) (dashed curves). The surface parameters were $H = 0.7$ and $l = 10^{-4}\lambda$ [$s(\lambda) = 0.063$] with $\lambda = 612.7\,\text{nm}$. The angles of the incident light were 0° and 50° as indicated in the figure.

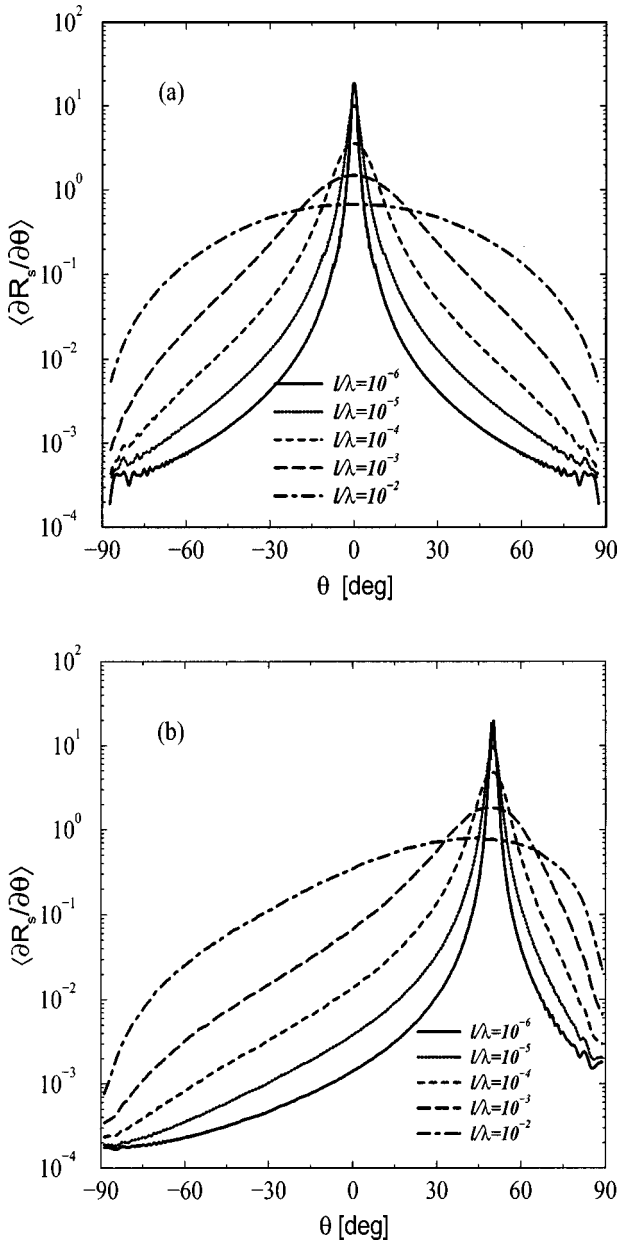


Fig. 5. Same as Figs. 2 (single-scattering results), but now with a rigorous numerical-simulation approach (see text for details) that incorporates all higher-order scattering processes.

cases $H = 0.7$, while for the angles of incidence we used $\theta_0 = 0°$ [Fig. 5(a)] and $\theta_0 = 50°$ [Fig. 5(b)]. The height standard deviation as measured over the whole length of the surface, $L = 100\lambda$, according to Eq. (3) ranged from $\sigma(L) = 0.4\lambda$ for the smallest topothesy up to as large as $6.3\lambda$ for the largest. The fact that we did not really use the total length $L$ during the surface generation when adjusting the topothesy but instead used a slightly smaller fraction of this length did not seem to affect the height standard deviation to a large degree. In fact, it was found numerically that the RMS heights of the generated surfaces were only a few percent lower than the one obtained from using Eq. (3), and we will therefore in the following use this equation in estimating the RMS height of the surfaces. According to optical criterion these surface roughnesses correspond to rather rough surfaces. In particular, one observes from Fig. 5 that in the case of $l = 10^{-2}\lambda$ a specular peak is hard to define at all in the mean DRC spectra. This is a clear indication of a highly rough surface and thus a very severe test of our theory.

To further compare the analytic results derived earlier with those obtained from the numerical simulation approach, in Fig. 6 we have plotted the amplitude of the specular peaks (circles) $\langle \partial R_s/\partial\theta \rangle|_{\theta=\theta_0}$ and their widths (squares) $w(H, l/\lambda, \theta_0)$, as obtained from the numerical simulation results shown in Fig. 5. The solid lines of this figure are the analytic predictions for these quantities as given respectively by relations (20) and (21). As can be seen from this figure, the analytic predictions are in excellent agreement with their numerical simulation counterparts. In particular this confirms the decaying and the increasing power laws in topothesy of the exponent $1/H - 1$ for these two quantities, respectively.

From Eqs. (17) we observe that if we replot the mean DRC times the inverse of the prefactor of the Lévy distribution versus its argument, all mean DRC curves corresponding to the same Hurst exponent should (within single scattering) collapse onto one and the same master curve. This master curve should be the Lévy distribution, $\mathcal{L}_{2H}(x)$, of order $2H$. Notice that this data collapse should hold true for arbitrary values for the angle of incidence and topothesy. The failure of such a data collapse (onto $\mathcal{L}_{2H}$) indicates essential contributions from multiple-scattering effects. The range of scattering angles where such processes are important can therefore be read off from such a plot. Furthermore, since the tails of the Lévy distribution $\mathcal{L}_{2H}(x)$ drop off as $x^{-2H-1}$ [see Eq. (23)], such rescaled mean DRC plots can be used to measure the Hurst exponent of the underlying self-affine surfaces for which the light-scattering data have been ob-

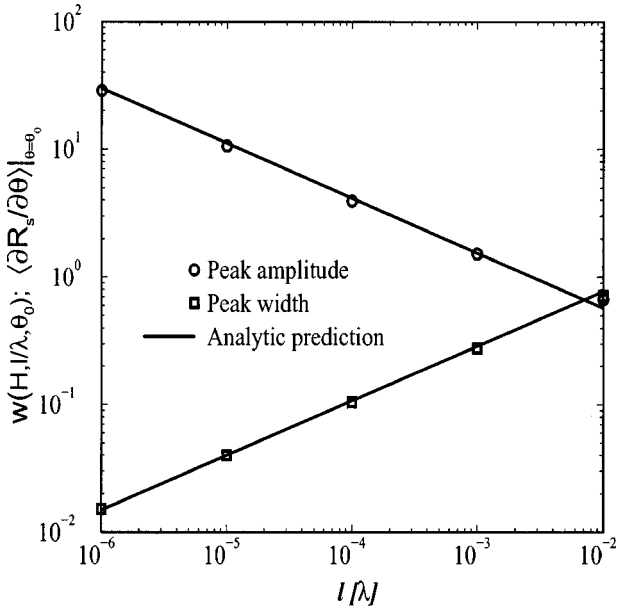


Fig. 6. Specular peak amplitude, $\langle \partial R_s/\partial\theta \rangle|_{\theta=\theta_0}$, and its half-width at half-maximum, $w(H, l/\lambda, \theta_0)$ as a function of topothesy $l$. The angle of incidence was in both cases $\theta_0 = 0°$. The solid lines are analytical results obtained from relations (20) and (21), and the circles (amplitudes) and the squares (widths) were obtained from the numerical simulations results shown in Fig. 5(a).

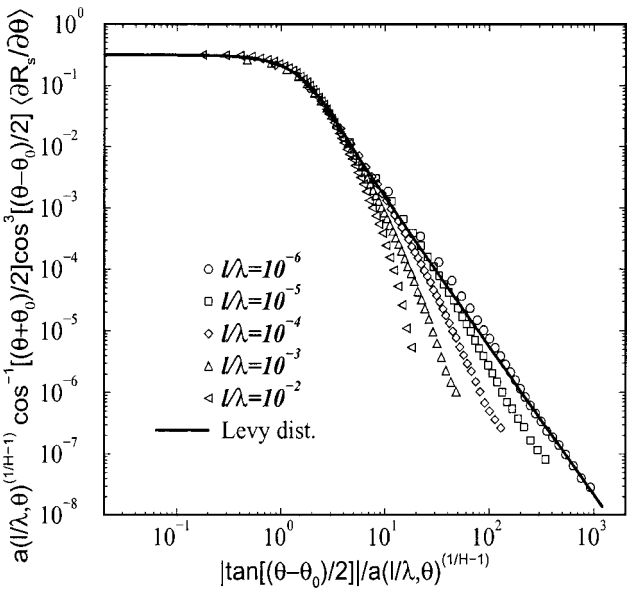


Fig. 7. Rescaled version of the rigorous numerical-simulation results shown in Fig. 5(b). Only the data corresponding to $\theta < 50°$ are included. In the rescaled coordinates all data (symbols) should within the single-scattering approximation collapse onto a Lévy distribution of order $2H$ (solid curve).

tained. To check these predictions for our numerical-simulation results, we present in Fig. 7 such a rescaling of the data originally presented in Fig. 5(b). Only data lying to the left of the specular peak have been included, i.e., only data for scattering angles $\theta < \theta_0 = 50°$. As can be seen from this figure, the various scattering curves fall nicely onto the master curve (solid curve) in regions where single scattering is dominating. When multiple-scattering processes start making a considerable contribution, the scattering curves start to deviate from this master curve. This observation could be used in practical applications to determine for what regions the scattering is dominated by single-scattering processes. For the lowest topothesy considered here, $l = 10^{-6}\lambda$, a power law extends nicely over large regions of scattering angles—a signature of the diffuse scattering from self-affine surfaces. According to relation (24) the exponent of this power law should be $-1 - 2H$. A regression fit to the scattering curve corresponding to the topothesy $l = 10^{-6}\lambda$ gives $H = 0.73 \pm 0.02$, where the error indicated is a pure regression error. The real error is of course larger. With the knowledge of the Hurst exponent obtained from the decay of the diffuse tail of the mean DRC, we might now, on the basis of the amplitude of the specular peak, obtain an estimate of the topothesy of the surface. From the numerical simulation result we have that $\langle \partial R_s/\partial\theta\rangle|_{\theta=\theta_0} \simeq 17.9$, which together with relation (20) gives $l = 0.97 \times 10^{-6}\lambda$, where we have used the value found above for the Hurst exponent. These two results fit quite nicely with the values $H = 0.7$ and $l = 10^{-6}\lambda$ used in the numerical generation of the underlying self-affine surfaces.

It should be noticed that for the numerical results presented in this paper, we have not considered topothesies smaller than $l = 10^{-6}\lambda$. However, since, as also indicated by our numerical results, lowering the topothesy will favor single-scattering processes over those obtained from multiple scattering, the analytic results [Eqs. (17)] will trivially be valid for low values of the topothesy. This has also been checked explicitly by numerical simulations (results not shown).

So far in this paper we have assumed that the metal was a perfect conductor. Obviously this is an idealization, and even the best conductors known today are not perfect conductors at optical wavelengths. By relaxing the assumption of the metal being perfectly conducting to instead being a good conductor, i.e., a real metal, we are no longer in position to obtain a closed-form solution of the scattering problem, the reason being that the boundary conditions are no longer local quantities. In this case we therefore have to resort to numerical calculations. In order to see how well our analytic results [Eqs. (17)] describe the scattering from real metals (in contrast to perfect conductors), in Fig. 8 we give the mean DRC, as obtained from numerical simulations,[36] for a self-affine silver surface of Hurst exponent $H = 0.7$ and topothesy $l = 10^{-4}\lambda$. We recall that this choice for the topothesy corresponds to a rather rough surface where the RMS height measured over the whole length of the surface is $\sigma(L) \sim 1.45\lambda$. Furthermore, the angles of incidence were $\theta = 0°$ and 50°, and the wavelength of the incident light was $\lambda = 612.7$ nm. At this wavelength the dielectric constant of silver is $\varepsilon(\omega) = -17.2 + 0.50i$.[44] The dashed curves of Fig. 8 represent the predictions from Eqs. (17), and as can be seen from this figure, the correspondence is rather good. It is interesting to see that the agreement between the analytical and the numerical results is of the same quality as that found for the perfect conductor [see Fig. 4(b)]. This indicates that the analytic results given by Eqs. (17) are rather robust and tend also to describe well the scattering from a good, but not necessarily perfect, reflector. Simulations equivalent to those reported for silver have also been performed for alumi-

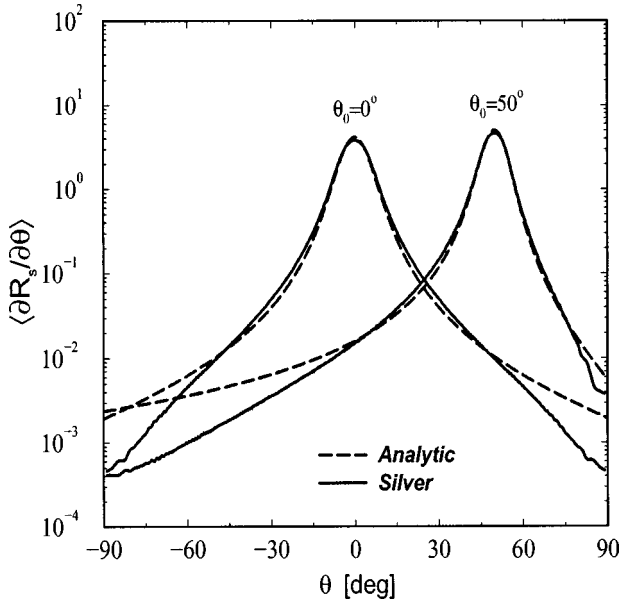


Fig. 8. Same as Fig. 4(b), but now with a real metal (silver) instead of a perfect conductor. The value of the dielectric constant of silver at the wavelength of the incident light ($\lambda = 612.7$ nm) was $\varepsilon(\omega) = -17.2 + 0.50i$.

num (results not shown), which has a dielectric function that is more than three times higher at the wavelength ($\lambda = 612.7\,\mathrm{nm}$) used here. The conclusions found above for silver also hold true for aluminum. We find it interesting to note that such self-affine aluminum surfaces were recently reported to be seen for cold rolled aluminum.[17] The Hurst exponents were measured to be $H = 0.93 \pm 0.03$ and $H = 0.50 \pm 0.05$ for the transverse and longitudinal directions, respectively.

Before closing this section we would like to mention that for real metals the numerical-simulation approach based on Eq. (25a) and used above can no longer be used directly. Instead, a coupled set of inhomogeneous Fredholm integral equations of the second type has to be solved for the electric field, which is nonzero on the surface of a real metal, and its normal derivative divided by the dielectric constant of the metal. Details of this approach can be found in, for example, Ref. 36.

## 6. CONCLUSIONS

We have considered the scattering of *s*-polarized plane incident electromagnetic waves from randomly rough self-affine metal surfaces characterized by the roughness exponent $H$ and the topothesy $l$ [or slope $s(\lambda)$]. By considering perfect conductors, we derived within the Kirchhoff approximation a closed-form solution for the mean differential reflection coefficient in terms of the parameters characterizing the rough surface—the Hurst exponent and the topothesy (or slope)—and the wavelength and the angle of incidence of the incident light. These analytic predictions (written from a Lévy distribution of index $2H$) were compared against results obtained from extensive, rigorous numerical simulations based on the extinction theorem. An excellent agreement was found over large regions of parameter space. Finally, the analytic results, valid for perfect conductors, were compared with numerical-simulation results for a (nonperfectly conducting) silver self-affine surface. It was demonstrated that also in this case the analytic predictions gave quite satisfactory results even though strictly speaking they were outside their region of validity.

## ACKNOWLEDGMENTS

The authors thank Jean-Jacques Greffet, Tamara Leskova, and Alexei A. Maradudin for useful comments about this work. I. Simonsen thanks the Research Council of Norway (contract No. 32690/213), Norsk Hydro ASA, Total Norge ASA, and the Centre National de la Researche Scientifique for financial support.

Corresponding author Damien Vandembroucq's e-mail address is damien.vandembroucq@saint-gobain.com.

## REFERENCES

1. J. W. S. Rayleigh, *The Theory of Sound* (Dover, New York, 1945).
2. M. Nieto-Vesperinas and J. M. Soto-Crespo, "Monte Carlo simulations for scattering of electromagnetic waves from perfectly conductive random rough surfaces," Opt. Lett. **12**, 979–981 (1987).
3. E. R. Méndez and K. A. O'Donnell, "Observation of depolarization and backscattering enhancement in light scattering from Gaussian random rough surfaces," Opt. Commun. **61**, 91–95 (1987).
4. A. A. Maradudin, E. R. Méndez, and T. Michel, "Backscattering effects in the elastic scattering of *p*-polarized light from a large-amplitude random metallic grating," Opt. Lett. **14**, 151–153 (1989).
5. J. A. Sanchez-Gil, "Coupling, resonance transmission, and tunneling of surface-plasmon polaritons through metallic gratings of finite length," Phys. Rev. B **53**, 10317–10327 (1996).
6. S. C. Kitson, W. L. Barnes, and J. L. Sambles, "Full photonic band gap for surface modes in the visible," Phys. Rev. Lett. **77**, 2670–2673 (1996).
7. F. Pincemin and J. J. Greffet, "Propagation and localization of a surface plasmon polariton on a finite grating," J. Opt. Soc. Am. B **13**, 1499–1509 (1996).
8. J. A. Sanchez-Gil and A. A. Maradudin, "Competition between Anderson localization and leakage of surface-plasmon polaritons on randomly rough periodic metal surfaces," Phys. Rev. B **56**, 1103–1106 (1997).
9. C. S. West and K. A. O'Donnell, "Observation of backscattering enhancement from polaritons on a rough metal surface," J. Opt. Soc. Am. A **12**, 390–397 (1995).
10. A. Sentenac and J. J. Greffet, "Mean-field theory of light scattering by one-dimensional rough surfaces," J. Opt. Soc. Am. A **15**, 528–532 (1998).
11. S. L. Broschat and E. I. Thorsos, "An investigation of the small slope approximation for scattering from rough surfaces. i: theory," J. Acoust. Soc. Am. **97**, 2082–2093 (1995).
12. J. A. Ogilvy, *Theory of Wave Scattering from Random Rough Surfaces* (IOP, Bristol, UK, 1991).
13. P. Beckmann and A. Spizzichino, *The Scattering of Electromagnetic Waves from Rough Surfaces* (Artech House, Norwood, Mass., 1963).
14. B. B. Mandelbrot, *The Fractal Geometry of Nature* (Freeman, New York, 1975).
15. E. Bouchaud, "Scaling properties of cracks," J. Phys. Condens. Matter **9**, 4319–4344 (1997).
16. P. Meakin, *Fractals, Scaling and Growth Far from Equilibrium* (Cambridge U. Press, Cambridge, UK, 1998).
17. F. Plouraboué and M. Boehm, "Multi-scale roughness transfer in cold metal rolling," Tribol. Int. **32**, 45–57 (1999).
18. M. V. Berry, "Diffractals," J. Phys. A **12**, 781–797 (1979).
19. D. L. Jaggard and X. Sun, "Fractal surface scattering: a generalized Rayleigh solution," J. Appl. Phys. **68**(11), 5456–5462 (1990).
20. M. K. Shepard, R. A. Brackett, and R. E. Arvidson, "Self-affine (fractal) topography: surface parametrization and radar scattering," J. Geophys. Res. **100**, E6, 11709–11718 (1995).
21. P. E. McSharry, P. J. Cullen, and D. Moroney, "Wave scattering by a two-dimensional band limited fractal surface based on a perturbation of the Green's function," J. Appl. Phys. **78**(12), 6940–6948 (1995).
22. N. Lin, H. P. Lee, S. P. Lim, and K. S. Lee, "Wave scattering from fractal surfaces," J. Mod. Opt. **42**, 225–235 (1995).
23. J. Chen, T. K. Y. Lo, H. Leung, and J. Litva, "The use of fractals for modeling EM waves scattering from rough sea surface," IEEE Trans. Geosci. **34**(4), 966–972 (1996).
24. C. J. R. Sheppard, "Scattering by fractal surfaces with an outer-scale," Opt. Commun. **122**, 178–188 (1996).
25. J. A. Sánchez-Gil and J. V. García-Ramos, "Far field intensity of electromagnetic waves scattered from random, self-affine fractal metal surfaces," Waves Random Media **7**, 285–293 (1997).
26. J. A. Sánchez-Gil and J. V. García-Ramos, "Calculations of the direct electromagnetic enhancement in surface enhanced raman scattering on random self-affine fractal metal surfaces," J. Chem. Phys. **108**, 1317–1325 (1998).
27. Y-P Zhao, C. F. Cheng, G. C. Wang, and T. M. Lu, "Power law behavior in diffraction from fractal surfaces," Surf. Sci. **409**, L703–L708 (1998).
28. E. Jakeman, "Scattering by fractals" in *Fractals in Physics*,

L. Pietronero and E. Tossati, eds. (Elsevier, Amsterdam, 1986), pp. 55–60.
29. D. L. Jordan, R. C. Hollins, E. Jakeman, and A. Prewett, "Visible and infra-red scattering from well-characterized surfaces," Surf. Topog. **1**, 27–36 (1988).
30. H. N. Yang, T. M. Lu, and G. C. Wang, "Diffraction from surface growth fronts," Phys. Rev. B **47**, 3911–3922 (1993).
31. Y. P. Zhao, G. C. Wang, and T. M. Lu, "Diffraction from non-Gaussian rough surfaces," Phys. Rev. B **55**, 13938–13952 (1997).
32. Y. P. Zhao, I. Wu, C. F. Cheng, U. Block, G. C. Wang, and T. M. Lu, "Characterization of random rough surfaces by in-plane light scattering," J. Appl. Phys. **84**, 2571–2582 (1998).
33. I. Simonsen, D. Vandembroucq, and S. Roux, "Wave scattering from self-affine surfaces," Phys. Rev. E **61**, 5914–5917 (2000).
34. J. Schmittbuhl, J. P. Vilotte, and S. Roux, "Reliability of self-affine measurements," Phys. Rev. E **51**, 131–147 (1995).
35. I. Simonsen, A. Hansen, and O. M. Nes, "Determination of Hurst exponents by use of the wavelet transform," Phys. Rev. E **58**, 2779–2787 (1998).
36. A. A. Maradudin, T. Michel, A. R. McGurn, and E. R. Méndez, "Enhanced backscattering of light from a random grating," Ann. Phys. (New York) **203**, 255–307 (1990).
37. P. Lévy, *Théorie de l'Addition des Variables Aléatoires* (Gauthier-Villars, Paris, 1937).
38. B. V. Gnedenko and A. N. Kolmogorov, *Limit Distributions for Sum of Independent Random Variables* (Addison Wesley, Reading, Mass., 1954).
39. E. I. Thorsos, "The validity of the Kirchhoff approximation for rough surface scattering using a Gaussian roughness spectrum," J. Acoust. Soc. Am. **83**, 78–82 (1988).
40. E. I. Thorsos and D. R. Jackson, "Studies of scattering theory using numerical methods," Waves Random Media **3**, S165–S190 (1991).
41. M. Abramowitz and I. A. Stegun, *Handbook of Mathematical Functions* (Dover, New York, 1964).
42. W. H. Press, S. A. Teukolsky, W. T. Vetterling, and B. P. Flannery, *Numerical Recipes*, 2nd ed. (Cambridge U. Press, Cambridge, UK, 1992).
43. J. Feder, *Fractals* (Plenum, New York, 1988).
44. E. D. Palik, *Handbook of Optical Constants of Solids* (Academic, New York, 1985).